Liner impedance determination from PIV acoustic measurements

Antoni Alomar, Yves Aurégan
LAUM-CNRS, Universite du Maine, Le Mans, France.

Summary
An indirect method to determine the impedance of a locally reacting liner in absence of flow is presented, based on Particle Image Velocimetry. An error function is defined which quantifies the difference between the measured and computed velocity fields, and whose minimum corresponds to the optimum impedance and incoming plane wave amplitude. It is expressed in terms of either single phase velocity fields or the Fourier amplitude, leading to different optimum impedances. It is shown that the impedances obtained from single phase measurements are subject to a larger error than the ones obtained from Fourier amplitudes or from their average along a period. The error is attributed to weak convection effects due to the background flow needed to sustain the seeding particles.

PACS no. xx.xx.Nn, xx.xx.Nn

1. Introduction

During the last decades there is an increasing interest in diminishing comunity noise. In a joint effort between academia and industry, the sources of sound involved are investigated, together with means for their reduction and control. In many situations, sound is generated and propagated through pipes or ducts. In that situation, acoustic liners are designed and commonly used to attenuate the noise levels. The most well-known application are aircraft aero-engines, whose inner walls are treated with liners to attenuate the noise generated by the fan and the combustion chamber.

A particular type of liners are the so-called locally reacting liners, where the interaction of the acoustic field with the lined wall is local, i.e. the impedance boundary condition is defined locally. If the liner is also linear (the boundary condition is independent of the incident sound amplitude and incidence) the boundary condition can be reduced to a single value of the acoustic impedance, at a given frequency. This is actually the boundary condition needed by an acoustic solver in absence of grazing flow. When there is flow the boundary condition changes [1], although still involves the liner impedance as defined above.

Several methods are used to determine the liner impedance. In the so-called direct methods, the impedance is calculated exclusively from microphone measurements. The *in situ* method consists of fixing the microphones inside the liner cavities, in order to measure directly the pressure and velocity inside the liner [2]. It has two important drawbacks: it is intrusive, and it can only determine the local cavity impedance. The well-known two-microphone method is used in normal incidence tubes, and therefore cannot be used with grazing flow over the liner [3, 4].

More convenient have been found to be the indirect methods, which make use of the computed acoustic field together with experimental data to determine the liner impedance. The single mode method [5] uses the simplifying assumption that a single mode is propagating along the lined section, which provides an analytical solution, but it's accuracy is limited. More recent methods use a more accurate numerical description of the acoustic field, using the finite element method [6, 7, 8] or modal methods [9, 10, 11] as acoustic solvers. Most of the experimental data used in the past consists of microphone measurements along the duct, but also laser doppler velocimetry (LDV) has been used [12, 13].

A measurement technique which has not been applied to liner impedance eduction despite having a potential advantage is particle image velocimetry (PIV). PIV has been successfully used in the past to measure the acoustic particle velocity in a number of other applications within acoustics, and its capabilities and limitations are well established [14]. The reason for using PIV is that, as opposed to microphones and LDV, it provides the acoustic field simultaneously on an entire plane, from a single measurement. To obtain the same amount of spatial information with LDV, a huge number of successive measurements would be needed (of the order of thousands). The information

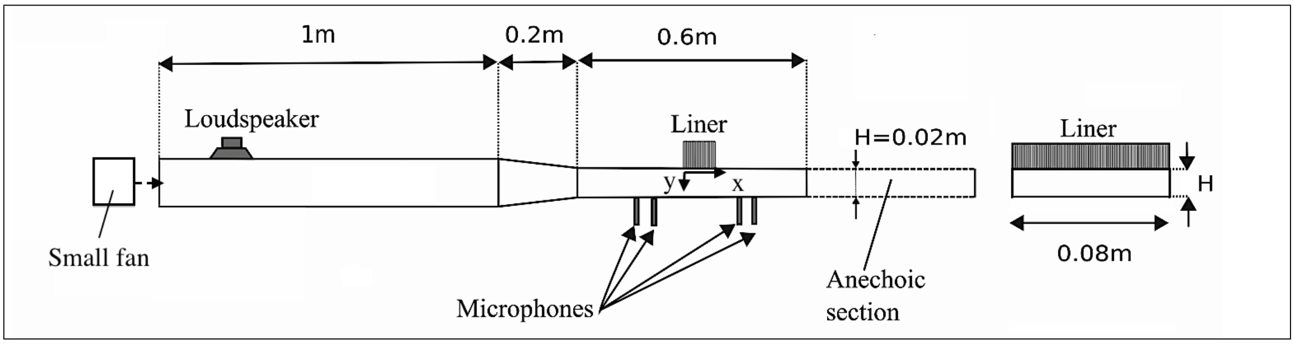

Figure 1. Experimental setup [15].

contained in the velocity fields may lead to a sharper and less error sensitive impedance eduction.

2. Experimental setup

The rig used consists of a rectangular duct with cross section dimensions of 8 cm (width) $\times$ 2 cm (height). The test section is 0.6 m long, and has an anechoic termination. The lined wall is located at the centre of the test section. It spans the entire channel width and has a length of 8 cm. The test section has two rectangular windows, one on the opposite wall to the liner and another at a side wall. The former lets the laser sheet pass through, illuminating the entire lined section, and the latter allows the light reflected to reach the camera. In order to use PIV, a uniform distribution of seeding particles are required to fill the channel. For the present case of no mean flow this is difficult to achieve, and a small amount of ventilation was needed. A small fan was fixed at the duct inlet which generated a low flow velocity and allowed a proper distribution of particles. The velocity at the centreline was 0.5 m/s, corresponding to a Reynolds number of 640. The incoming sound is generated by a loudspeaker fixed immediately downstream of the channel inlet. The sound level was close to the maximum allowed by the amplifier, in order to maximise the signal-to-noise ratio. The same rig was used by Marx *et al.* [15], and it is sketched in Figure 1.

The liner is of honeycomb-type, with high porosity and low resistivity. It consists of a set of metallic, hexagonal, rigidly terminated cavities with a depth of 5 cm and diameter of 2 mm. The resonance frequency of the liner is 1700 Hz. An impedance model based on a time domain formulation [16] has been considered for comparison:

$$\frac{Z}{\rho_o c_o} = -\frac{i}{\phi}\cot(\frac{D\omega}{c_e} - \frac{i\epsilon}{2}), \quad (1)$$

where $\phi = 0.9$ is the porosity, $D = 5$ cm is the liner depth, ρ_o is the ambient air density, c_o is the ambient sound speed, and c_e and ϵ are model parameters.

An upstream and a downstream pair of microphones flush to the wall were used to measure the

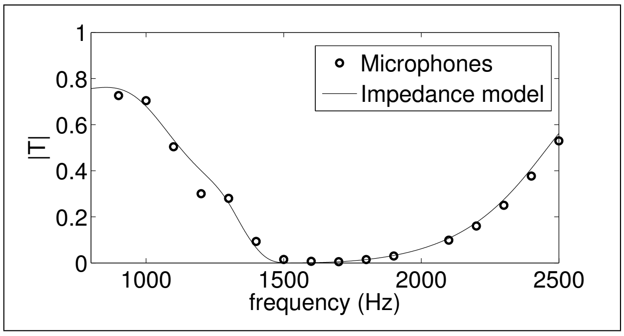

Figure 2. Measured transmission coefficient and computed from equation 1.

upstream and downstream plane wave amplitudes and the scattering matrix. The distance between the microphones in each pair is 8.5 cm. The upstream microphone of the upstream pair is located at $x = -17$ cm, and the upstream microphone of the downstream pair at $x = 17$ cm (axis origin is on the liner upstream edge).

The impedance model parameters, including the porosity, were determined by a best-fit of the measured transmission and reflection coefficients in the frequency range of interest (see Figure 2). The obtained parameter values are $\phi = 0.91$, $c_e = 331$ and $\epsilon = 0.17$. In the vicinity of the resonant frequency significant nonlinear effects were detected in the downstream microphone signals.

A Dantec PIV system has been used. It consists of a Litron laser pulse generator of 532 nm, synchronised with a high-speed FlowSenseEO 29M camera, of 6600$\times$4400 pixels. The time between images was 200 μs, and the time between image pairs 0.5 s. An adaptive correlation algorithm provided by the Dantec software was used, which increased the image pairs cross-correlation, reaching a window size of 32$\times$32 pixels. To increase the resolution, an overlap of 50% was used.

The PIV plane is shown in Figure 3. To eliminate errors from merging adjacent vector fields, the entire lined section was captured from a single snapshot. This caused the aspect ratio of the PIV plane to be large, and the number of pixels along the chan-

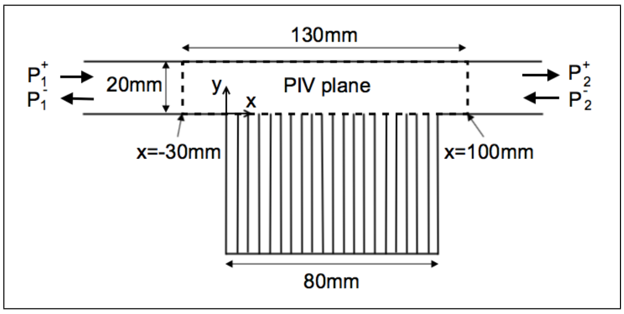

Figure 3. PIV plane.

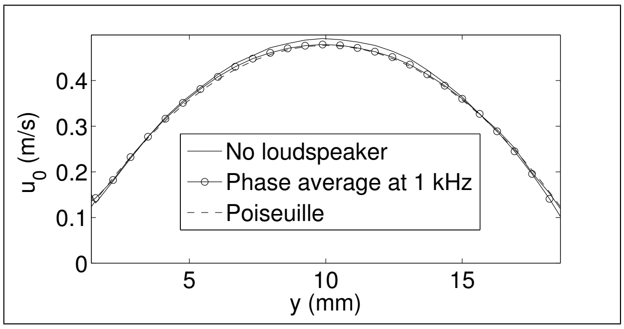

Figure 4. Mean velocity profile measured at $x = -10$ mm, together with the Poiseuille profile.

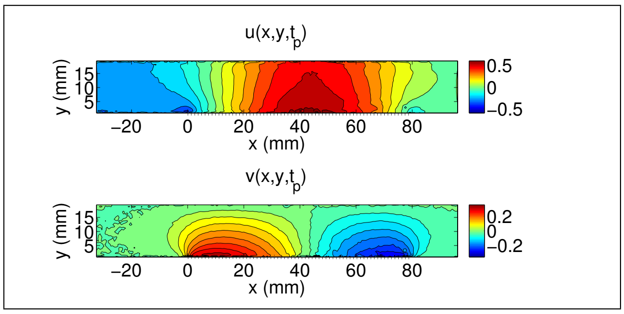

Figure 5. Instantaneous streamwise and wall-normal velocity contours corresponding to the phase 0° and 1 kHz.

nel height was limited to 610. Finally, the PIV plane contained 233 (streamwise)×32 (wall-normal) vectors. Each velocity vector field was obtained by averaging at least 100 instantaneous velocity fields.

3. Velocity fields

The incoming sound are single-frequency plane waves. In this case, the Fourier amplitude is completely determined from two instantaneous velocity fields (if the phase difference between them is known). However, the obtained fields suffer from discontinuities induced by the inverse tangent function. This is avoided by using the conventional definition of the Fourier series for arbitrary periodic functions, although more single measurements are needed. Keeping only the fundamental component of the Fourier series, any acoustic magnitude can be expressed as:

$$q(x, y, t) = \mathrm{Re}(Q(x, y)\mathrm{e}^{i\omega t}), \quad (2)$$

$$Q(x, y) = \frac{2}{T}\int_0^T q(x, y, t)\mathrm{e}^{-i\omega t}\mathrm{d}t, \quad (3)$$

where q is any acoustic magnitude and Q is the fundamental complex Fourier coefficient, or Fourier amplitude. The velocity vector fields were measured at specified instants, determined by the delay with respect to the loudspeaker reference signal. At the frequencies 1 kHz and 1.7 kHz, eight vector fields were acquired, at uniformly distributed phases within a period. From these the Fourier amplitude can be computed from equation 3. At the rest of frequencies, only one velocity field was measured. Measurements without incoming sound were also performed. The experiments were performed during two independent testing campaigns, separated several months. Table I shows a summary of the measurements performed.

The mean velocity profiles measured with incoming sound (phase average along a period) and without incoming sound upstream of the liner are shown in Figure 4. They are close to each other and both fit well the Poiseuille profile.

Figure 5 shows an example of streamwise and wall-normal velocity contours (mean field subtracted) corresponding to the phase 0° at 1 kHz. An example of the signal measured at a point in time is shown in Figure 6. The fundamental Fourier component matches closely the measured signal. This is observed in all cases except for the streamwise velocity component at the resonance frequency, where it starts behaving nonharmonically at the fall-off region. At $x = 20-30$ mm the disagreement with the fundamental Fourier component is significant, as can be appreciated in Figure 7(a). However, the wall-normal component remains harmonic further downstream (Figure 7(b)). This fact points to unsteady convective flow more than acoustic nonlinear effects as the cause. It should be decreased by diminishing the mean convective velocity imposed by the small fan. But this is problematic because lower mean flow velocities prevent the seeding particles to be homogeneously distributed in the channel, especially close to the walls. The mean flow velocity used is actually close to the minimum that allows a uniform particle distribution, and no further decrease seems possible. If such unsteady flow is uncoupled of the acoustic field, but it has long characteristic times, it could be eliminated simply by increasing the acquisition time so that the slow unsteady currents are averaged out. Several measurements were performed with acquisition times of the order of five times the regular, and no clear improvement was detected. Further increasing of the acquisition time was discarded for practical reasons.

Table I. Velocity fields measured, labeled by the phase delay with respect to loudspeaker signal (a full period are 360°).

frequency (Hz)	Phases in campaign 1 (°)	Phases in campaign 2 (°)
750	-	0
1000	0, 45, 90, 135, 180, 225, 270, 315	0, 45, 90, 135, 180, 225, 270, 315
1250	-	0
1500	-	45
1700	0, 45, 90, 135, 180, 225, 270, 315	0, 45, 90, 135, 180, 225, 270, 315

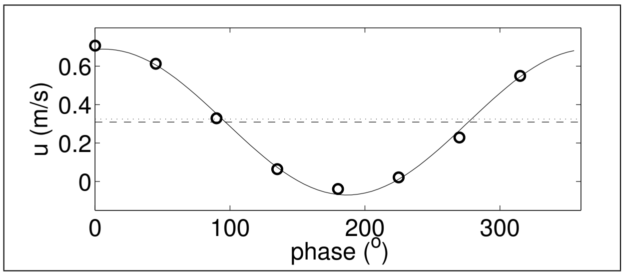

Figure 6. Streamwise velocity component measured at $(x, y) = (60, 4)$ mm, together with the fundamental Fourier component (line), the phase average (dashed) and no sound component (dotted).

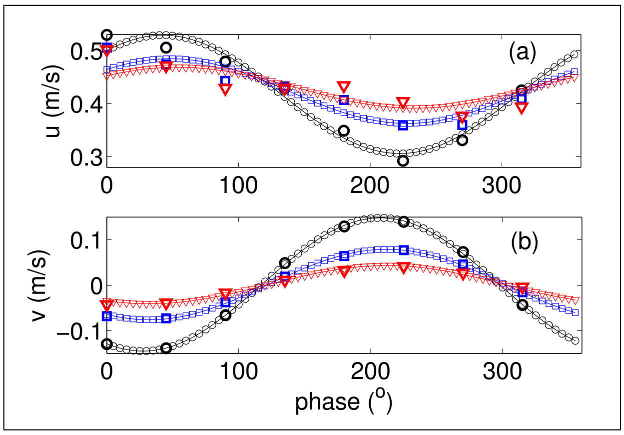

Figure 7. (a) Streamwise and (b) wall-normal velocity measured at $x = 20$ (black), 30 (blue) and 40 (red) mm, and $y = 4$ mm, for 1.7 kHz.

4. Error function and minimum search method

The liner impedance is determined by minimising an error function which quantifies the difference between the computed and measured velocity fields. The computed fields are obtained from a two-dimensional acoustic solver, based on a mixed multimodal-finite difference scheme. The three-zones method [9] is used to couple the hard and lined wall regions. The solver inputs are the liner impedance, Z, and the incoming plane wave amplitudes, P_1^+, P_2^-. It has been checked that the anechoic termination induces a small modulus of P_2^- in the frequency range of interest, and the effect of neglecting P_2^- on the optimum impedances is small. This fact, together with the significant increase in computation time when P_2^- is accounted for, has motivated the assumption $P_2^- = 0$ (perfectly anechoic termination).

In terms of the Fourier amplitudes, the following error function is considered:

$$\Psi = \sqrt{\frac{\iint_A |U_m(x,y) - U_c(x,y)|^2 \mathrm{d}x\mathrm{d}y}{\iint_A |U_m(x,y)|^2 \mathrm{d}x\mathrm{d}y}} + \sqrt{\frac{\iint_A |V_m(x,y) - V_c(x,y)|^2 \mathrm{d}x\mathrm{d}y}{\iint_A |V_m(x,y)|^2 \mathrm{d}x\mathrm{d}y}}, \tag{4}$$

where A is the PIV measurement area, and the subscripts 'm' and 'c' indicate that the quantity is measured or computed, respectively. It is remarked that this is one particular choice of error function. It could have been defined in terms of the velocity vector norm. The reason for treating separately U and V is that U is generally much bigger than V, and the resulting optimum values are close to the optimum values for U. In that case the misprediction of V is largely ignored. With the chosen function we give equal weight to both velocity components. The integrals are discretised using the grid from the PIV vector fields. In order to accelerate the computation time, the grid used is coarser than the PIV grid, containing 80 (streamwise)×13 (wall-normal) points.

When the single phase fields are used instead of the Fourier amplitude, $U_m(x, y)$ is replaced by the velocity field at the phase p considered, $u_m(x, y, t_p)$, and $U_c(x, y)$ is replaced by the real component of the Fourier amplitude, $\mathrm{Re}(U_c(x, y))$.

To find the minimum of the error function, a simple iterative procedure has been adopted, which consists of a moving grid of the independent variables, with decreasing size. The minimum of each grid is used as the centre of the following grid, and when the grid centre is repeated, the grid size is decreased. This procedure is repeated until a convergence criteria is fulfilled. The number of grid points per variable has been limited to five. More grid points start to increase the computation time. Several cases have been checked against the gradient descent algorithm, obtaining the same result.

5. Results

The real and imaginary components of the educed impedances at 1 kHz and 1.7 kHz are shown in Figures 8(a-b) and Figures 8(c-d), respectively. In addition to the values educed from the single phases (solid) and from the Fourier amplitudes (dashed), the phase average of the former are shown (dotted). Significant variability exists between the values obtained from the single phase measurements in all cases, as well as between the two testing campaigns. No clear correlation of the educed impedances with the phase is appreciated. When looking to the values obtained from the Fourier amplitudes and the phase average, the variability is lower between the different campaigns.

The variability is somewhat higher at 1.7 kHz. At this frequency the acoustic velocity diminishes to values close to zero at about half the liner length, while on the upstream liner half, the velocity signal is approximately in phase, and it goes to zero everywhere simultaneously. In this phase range the signal-to-noise ratio increases, and also the error in the educed impedance. Furthermore, at this frequency non-harmonic behaviour was detected in the streamwise velocity field, as discussed in Section 3. It is therefore important, if the impedance needs to be determined from a single phase, that it doesn't correspond to weak velocities.

Figure 9 shows the optimum impedances as a function of frequency. The impedances at 1 kHz and 1.7 kHz are the ones obtained from the Fourier amplitude. Good agreement with the impedance model is observed, with the exception of the resistance at low frequencies. This can be partly due to error in the impedance model parameters, as nonlinear effects were important around the resonance frequency.

Figure 10 shows the error function contours at 1.7 kHz based on (a) Fourier amplitude, (b) single phase 0° and (c) single phase 45°. The incoming plane wave amplitude is fixed to the optimum. It is appreciated that, not only the optimum impedance, but also the shape of the basin containing the minimum is different in the three cases. While in (a) the minimum is the centre of an approximately symmetric basin, in (b) and (c) the basins are deformed in certain directions. The shape of the error function depends on the experimental error, but also on the particular choice of error function. In absence of experimental error, different error functions can have different basin shapes, but must have the same minimum location. Different error functions can have associated minimum locations more or less sensitive to the measurement error. This includes changing the region of integration on the PIV plane, or how the different velocity components are treated. In other words, the choice of error function and integration region can be also optimised to minimise the error of the educed impedance. This is left as future work.

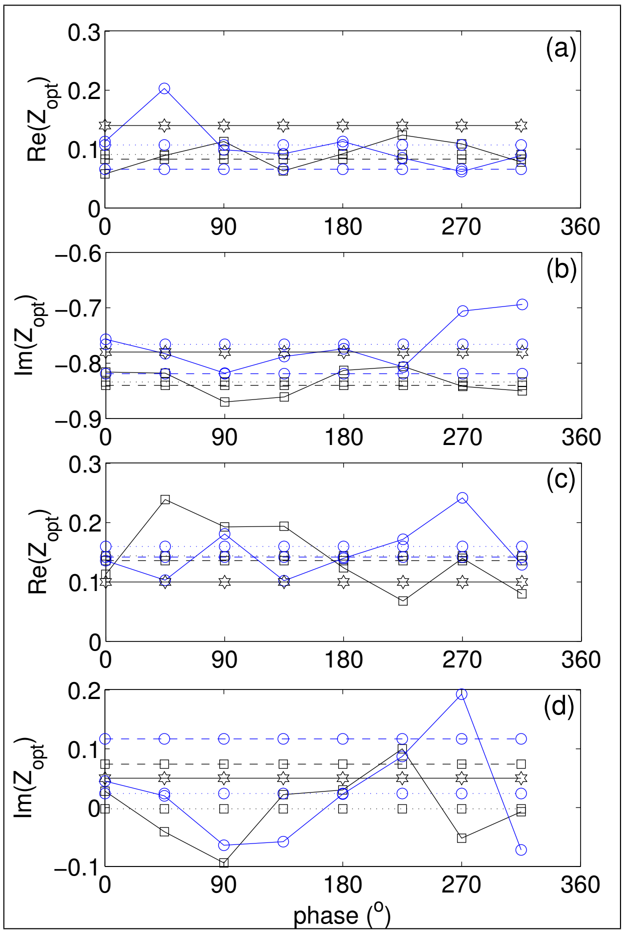

Figure 8. Liner impedances at (a,b) 1 kHz and (c,d) 1.7 kHz (solid: from single phases, dashed: from Fourier amplitude, hexagons: from impedance model, circles: first testing campaign, squares: second testing campaign).

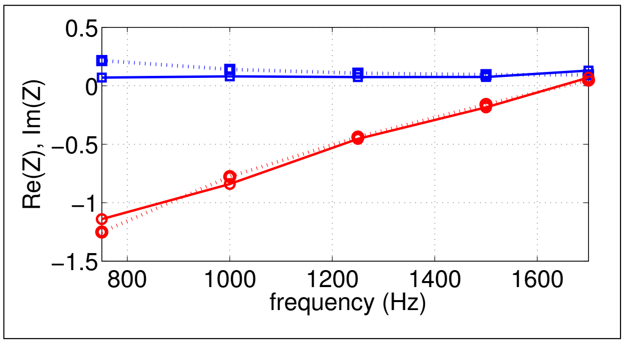

Figure 9. Real and imaginary components of the optimum (solid) and model (dotted) liner resistances (squares) and reactances (circles).

6. CONCLUSIONS

The method presented has been shown to determine the impedance of a locally reacting liner with reasonable accuracy, for frequencies up to resonance. The error is greater when the impedance is educed from single phase velocity fields, and it is lower when using the Fourier amplitude, or simply an average of the

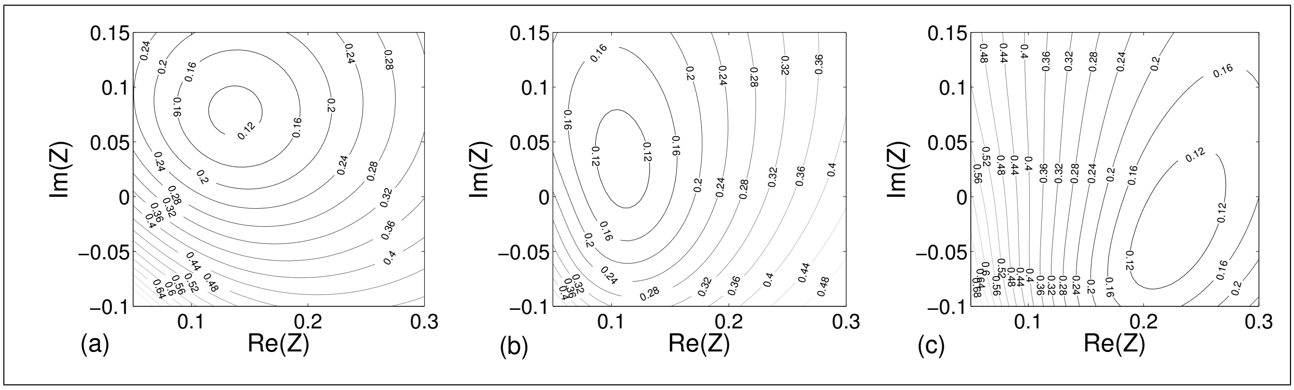

Figure 10. Contour levels of the error function at 1.7 kHz based on (a) the Fourier amplitude, (b) the single phase 0°, and (c) the single phase 45°, with the incoming plane wave amplitude fixed to the optimum.

impedances educed from single phases. The random component of the results suggests that the accuracy will increase when increasing the number of phases per period.

This experimental, random error has been tentatively attributed to unsteady, streamwise convective currents, which might be coupled with the acoustic field. They are caused by the background convective flow needed to sustain the seeding particles uniformly distributed. They are therefore difficult to eliminate in the present configuration. The error is somewhat higher around the resonance frequency. A reason for this is that, at the resonance, the velocity becomes low everywhere simultaneously in certain phase ranges, diminishing the signal-to-noise ratio.

The use of optimum error functions, i.e. ones that minimise the sensitivity of the educed impedance on the experimental error, can certainly lead to more accurate liner impedances.

Acknowledgement

This research is supported by the Marie Curie ITN FlowAirS. The authors would like to thank James Blondeau for his assistance during the tests.

References

[1] M. K. Myers: On the acoustic boundary condition in the presence of flow. Journal of Sound and Vibration 71 (1980) 429-434.

[2] P. Dean: An in situ method of wall acoustic impedance measurement in flow duct. Journal of Sound and Vibration 34 (1974) 97-130.

[3] J. Y. Chung, D. A. Blaser: Transfer function method of measuring in ducts acoustic properties, I-Theory. Journal of the Acoustical Society of America 68 (1980) 907-913.

[4] J. Y. Chung, D. A. Blaser: Transfer function method of measuring in ducts acoustic properties, II-Experiment. Journal of the Acoustical Society of America 68 (1980) 914-921.

[5] D. L. Armstrong, R. J. Beckermeyer, R. F. Olsen: Impedance measurements of acoustic duct liners with grazing flow. 87th Meeting of the Acoustical Society of America, New York, 1974.

[6] W.R. Watson, M.G. Jones, S.E. Tanner, T.L. Parrott: Validation of a numerical method for extracting liner impedance. AIAA Journal 34 (1996) 548-554.

[7] M. G. Jones, W. R. Watson, M. B. Tracy, T. L. Parrott: Comparison of two acoustic waveguides methods for determining liner impedance. 12th AIAA/CEAS Aeroacoustics Conference, Maastricht, Netherlands, 2001.

[8] J. Primus, E. Piot, F. Simon: An adjoint-based method for liner impedance eduction-validation and numerical investigation. Journal of Sound and Vibration 332 (2013) 58-75.

[9] Y. Aurégan, M. Leroux, V. Pagneux: Measurement of liner impedance with flow by an inverse method. 10th AIAA/CEAS Aeroacoustics Conference, Manchester, UK, 2004.

[10] T. Elnady, H. Boden: An analytical method for extracting liner impedance from measurements. 10th AIAA/CEAS Aeroacoustics Conference, Manchester, UK, 2004.

[11] M. Taktak, J. M. Ville, M. Haddar, G. Gabard, F. Foucart: An indirect method for the characterization of locally reacting liners. Journal of the Acoustical Society of America 127 (2010) 3548-3559.

[12] M. Lavieille, F. Simon, F. Micheli: Measurement of liner acoustic impedance in a shear layer of a subsonic flow by Laser Doppler Velocimetry. Symposium on the Acoustics of Poro-Elastic Materials (SAPEM), France, 2005.

[13] E. Piot, J. Primus, F. Simon: Liner impedance eduction technique based on velocity fields. 18th AIAA/CEAS Aeroacoustics Conference, Colorado Springs, CO, 2012.

[14] J.-C. Valière: Acoustic particle velocity measurements using lasers - Principles, signal processing and applications. Wiley, London, 2014.

[15] D. Marx, Y. Aurégan, H. Bailliet, J.-C. Valière: PIV and LDV evidence of hydrodynamic instability over a liner in a duct with flow. Journal of Sound and Vibration 329 (2010) 3798-3812.

[16] S.W. Rienstra: Impedance models in time domain, including the extended helmholtz resonator model. 12th AIAA/CEAS Aeroacoustics Conference, Cambridge, Massachusetts, 2006.